Frontiers of Physics
https://doi.org/10.1007/s11467-021-1056-y
Front. Phys.
16(4), 43502 (2021)

RESEARCH ARTICLE

Impurity effect as a probe for the pairing symmetry of graphene-based superconductors

Yuan-Qiao Li[1], **Tao Zhou**[2,3,1,†]

[1] *College of Science, Nanjing University of Aeronautics and Astronautics, Nanjing 210016, China*
[2] *Guangdong Provincial Key Laboratory of Quantum Engineering and Quantum Materials, School of Physics and Telecommunication Engineering, South China Normal University, Guangzhou 510006, China*
[3] *Guangdong–Hong Kong Joint Laboratory of Quantum Matter, Frontier Research Institute for Physics, South China Normal University, Guangzhou 510006, China*
Corresponding author. E-mail: [†] *tzhou@scnu.edu.cn*
Received January 19, 2021; accepted February 12, 2021

We study theoretically the single impurity effect on graphene-based superconductors. Four different pairing symmetries are discussed. Sharp in-gap resonant peaks are found near the impurity site for the $d+\mathrm{i}d$ pairing symmetry and the $p+\mathrm{i}p$ pairing symmetry when the chemical potential is large. As the chemical potential decreases, the in-gap states are robust for the $d+\mathrm{i}d$ pairing symmetry while they disappear for the $p+\mathrm{i}p$ pairing symmetry. Such in-gap peaks are absent for the fully gapped extended s-wave pairing symmetry and the nodal f-wave pairing symmetry. The existence of the in-gap resonant peaks can be explained well based on the sign-reversal of the superconducting gap along different Fermi pockets and by analyzing the denominator of the T-matrix. All of the features may be checked by the experiments, providing a useful probe for the pairing symmetry of graphene-based superconductors.

Keywords impurity effect, graphene, superconductivity

1 Introduction

The two-dimensional graphene material has been studied intensively for a long time [1, 2]. In particular, the realization of superconductivity in graphene has attracted considerable interest in the past decade. Experimentally, superconductivity was reported to be induced to the monolayer graphene growing on the superconducting Rhenium film [3]. Evidence of superconductivity was also observed on the Ca-intercalated bilayer graphene [4, 5], and the Li-decorated monolayer graphene [6]. And superconductivity in graphene can be induced through the proximity effect by placing it on an electron-doped cuprate superconductor. Quite interestingly, signatures of the p-wave pairing symmetry were observed through the scanning tunnelling spectroscopy (STS) investigation [7]. Recently, superconductivity was realized in the twisted bilayer graphene [8], which is the first pure-carbon-based two-dimensional superconductor.

On the theoretical side, the graphene was predicted to go into the superconducting state through doping or the proximity effect [9–21]. However, different pairing symmetries have been proposed by different groups. A chiral spin-triplet $p+\mathrm{i}p$ pairing symmetry was proposed based on an extended Hubbard model [13, 14]. A chiral $d+\mathrm{i}d$ pairing symmetry was proposed based on an exact numerical study [15], the renormalization group method [16–18] and the random phase approximation [19]. Recently, the $d+\mathrm{i}d$ pairing symmetry is also proposed to be the most favorable pairing symmetry in the twisted bilayer graphene [22, 23]. It was also proposed that the triplet f-wave pairing might occur under some particular conditions [17–19]. And an exotic s-wave pairing was proposed to be the favorable pairing symmetry in the bilayer graphene [20]. Therefore, so far there is no agreement about the preferred pairing symmetry in graphene-based superconductors. Actually, the pairing symmetry may depend strongly on the parameters, the starting model, the pairing mechanism and the approximation considered. Identifying the pairing symmetry is crucial to clarify microscopic details of the superconductivity. Especially, both the chiral superconductivity and the spin-triplet superconductivity are usually topologically nontrivial, thus the graphene material may provide a novel platform to study topological superconductors [24]. Therefore, now it is quite important to provide more detailed experimental information to resolve the pairing symmetry.

*arXiv: 1803.05841. This article can also be found at http://journal.hep.com.cn/fop/EN/10.1007/s11467-021-1056-y.

The impurity effect has been one powerful tool to explore the pairing symmetry of unconventional superconductors [25–32]. One prominent feature is the impurity induced in-gap resonant states in high-T_c cuprate superconductors [26]. This feature was used to identify the d-wave pairing symmetry [25, 26]. In iron-based superconductors, the existence of the impurity induced in-gap states was proposed to be a signature of the sign-reversal of the $s_{\pm}$-wave pairing gap [27, 28]. Theoretically, there are two effective methods to investigate the single impurity effect in the superconducting state. The first method is based on the Bogoliubov-de Gennes (BdG) equations. With this method the Hamiltonian in presence of an impurity is diagonalized numerically in the real space [32]. The second method is based on the self-consistent T-matrix method, with the Hamiltonian being expressed in the momentum space [26–31]. Previously, the impurity effect in the superconducting graphene has been studied based on these two methods [30–32]. With the T-matrix method, the impurity effect at a typical doping density was studied [30, 31]. Recently, based on the BdG technique, the impurity effect of graphene-based superconductors considering mainly the d-wave pairing symmetry was reported [32]. We note that so far a systematic study about the impurity effect in graphene-based unconventional superconductors based on the T-matrix method is still awaited and highly demanded. With the T-matrix method, the local density of states (LDOS) is expressed analytically and the origin of the impurity states can be explored numerically. Another advantage for the T-matrix method is that the Hamiltonian is expressed in the momentum space, so that there is no finite-size effect. The theoretical calculation of the LDOS can be compared with the STS experimental results directly so that the pairing symmetry may be distinguished [33–35].

Recently, it was reported experimentally that the graphene materials can be highly doped to beyond the Van Hove singularity filling [36, 38]. This experimental progress is of importance and may open a new door to study the possible superconductivity in graphene-based materials. Therefore, it is rather insightful to study systematically the single impurity effect of the possible superconducting state in the graphene lattice with different doping levels.

In the present work, we study theoretically the impurity effect of graphene-based superconductors based on the T-matrix method. Four different pairing symmetries, i.e., the $p+\mathrm{i}p$ pairing symmetry, the $d+\mathrm{i}d$ pairing symmetry, the extended s-wave pairing symmetry, and the f-wave pairing symmetry, are considered. For the cases of the extended s-wave and the f-wave pairing symmetries, no in-gap states are obtained. For the $p+\mathrm{i}p$ pairing symmetry, the results depend on the doping levels. As the chemical potential is large, there exist sharp resonant peaks for different impurity strengths. The resonant peaks disappear as the chemical potential decreases. For the $d+\mathrm{i}d$ pairing symmetry, the impurity induced in-gap peaks are robust and exist for all of the doping levels we considered. Our results indicate that the impurity effect may be useful to probe the pairing symmetry of graphene-based superconductors.

The rest of the paper is organized as follows. In Section 2, we introduce the model and derive the formalism. In Section 3, we report numerical calculations and discuss the obtained results. Finally, we present a brief summary in Section 4.

2 Model and Hamiltonian

For the honeycomb lattice describing the monolayer graphene, each unit cell contains two inequivalent lattice sites. The whole system includes two sublattices A and B. We start from a BCS-type Hamiltonian, including the nearest-neighbour hopping term, the chemical potential term, and the superconducting pairing term. Then the Hamiltonian is written as

$$H=\sum_{\boldsymbol{k}}\psi_{\boldsymbol{k}}^{\dagger}M_{\boldsymbol{k}}\psi_{\boldsymbol{k}}, \tag{1}$$

where the vector $\psi_{\boldsymbol{k}}^{\dagger}$ is expressed as

$$\psi_{\boldsymbol{k}}^{\dagger}=(A_{\boldsymbol{k}\uparrow}^{\dagger},B_{\boldsymbol{k}\uparrow}^{\dagger},A_{-\boldsymbol{k}\downarrow},B_{-\boldsymbol{k}\downarrow}). \tag{2}$$

$M_{\boldsymbol{k}}$ is a 4×4 matrix in the momentum space,

$$M_{\boldsymbol{k}}=\begin{pmatrix}-\mu & \gamma_{\boldsymbol{k}} & 0 & \Delta_{\boldsymbol{k}}\\ \gamma_{\boldsymbol{k}}^{*} & -\mu & \xi\Delta_{-\boldsymbol{k}} & 0\\ 0 & \xi\Delta_{-\boldsymbol{k}}^{*} & \mu & -\gamma_{\boldsymbol{k}}\\ \Delta_{\boldsymbol{k}}^{*} & 0 & -\gamma_{\boldsymbol{k}}^{*} & \mu\end{pmatrix}. \tag{3}$$

Here $\xi=1$ and -1 are for the spin singlet pairing symmetry and the spin triplet pairing symmetry, respectively. $\gamma_{\boldsymbol{k}}$ describes the nearest-neighbour electron hopping, with

$$\gamma_{\boldsymbol{k}}=-t\sum_{j=1,2,3}\mathrm{e}^{\mathrm{i}\boldsymbol{k}\cdot\boldsymbol{e}_j}, \tag{4}$$

with $\boldsymbol{e}_1=(1,0)$, $\boldsymbol{e}_2=\frac{1}{2}(-1,\sqrt{3})$, and $\boldsymbol{e}_3=\frac{1}{2}(-1,-\sqrt{3})$. $\Delta_{\boldsymbol{k}}$ represents the superconducting pairing function. Considering the electron pairing of the nearest-neighbour sites, it is expressed as,

$$\Delta_{\boldsymbol{k}}=\sum_{j=1,2,3}\Delta_j\mathrm{e}^{\mathrm{i}\boldsymbol{k}\cdot\boldsymbol{e}_j}. \tag{5}$$

Following Ref. [14], for the extended s-wave pairing symmetry and the f-wave pairing symmetry, we have $\Delta_j=\Delta_0(1,1,1)$. For the $p+\mathrm{i}p$ pairing symmetry and the $d+\mathrm{i}d$ pairing symmetry, we have $\Delta_j=\Delta_0(1,\mathrm{e}^{\mathrm{i}\frac{2}{3}\pi},\mathrm{e}^{\mathrm{i}\frac{4}{3}\pi})$.

We consider a single impurity being placed on the sublattice A in the unit cell $(0,0)$. The impurity Hamiltonian is written as

$$H_{imp} = V_s[A^{\dagger}_{(0,0),\uparrow}A_{(0,0),\uparrow} + A^{\dagger}_{(0,0),\downarrow}A_{(0,0),\downarrow}], \tag{6}$$

where V_s is the impurity strength. Then we can define the T-matrix as [26]

$$\hat{T}(\omega) = \hat{U}_0 \Big/ \left[\hat{I} - \hat{U}_0 \frac{1}{N}\sum_{\boldsymbol{k}} \hat{G}_0(\boldsymbol{k},\omega)\right]. \tag{7}$$

Here $\hat{I}$ is the 4×4 identity matrix. $\hat{G}_0(\boldsymbol{k},\omega)$ is the bare Green's function in the momentum space, with $\hat{G}_0(\boldsymbol{k},\omega)_{ij} = \sum_{n=1}^{4} \frac{u_{in}(\boldsymbol{k})u^{\dagger}_{nj}(\boldsymbol{k})}{\omega - E_n(\boldsymbol{k}) + i\delta}$. $u_{ij}(\boldsymbol{k})$ and $E_n(\boldsymbol{k})$ are obtained by diagonalizing the 4×4 Hamiltonian matrix of Eq. (3). The non-zero elements of the matrix $\hat{U}_0$ include $U_0^{11} = V_s$ and $U_0^{33} = -V_s$, respectively.

The LDOS is then expressed as

$$\rho(\boldsymbol{r},\omega) = -\frac{1}{\pi}\mathrm{Im}\mathrm{Tr}\hat{G}(\boldsymbol{r},\omega), \tag{8}$$

with

$$\hat{G}(\boldsymbol{r},\omega) = \hat{G}_0(0,\omega) + \hat{G}_0(\boldsymbol{r},\omega)\hat{T}(\omega)\hat{G}_0(-\boldsymbol{r},\omega). \tag{9}$$

The bare Green's function $\hat{G}_0(\boldsymbol{r},\omega)$ in the real space can be obtained by performing the Fourier transformation to the bare Green's function in the momentum space $\hat{G}_0(\boldsymbol{k},\omega)$.

In the results presented below, we use 1 eV as the energy unit. The nearest-neighbour hopping constant t is chosen as 2.7. The gap magnitude is usually very small in real materials. In the present work, as usually done, we consider a much larger inputting gap to make the detailed in-gap features clear. Our main results do not change qualitatively with different gap magnitudes.

3 Results and discussion

The normal state energy bands [obtained by setting $\Delta_{\pm\boldsymbol{k}} = 0$ in Eq. (3)] along the highly symmetrical lines in the Brillouin zone are plotted in Fig. 1(a). As is seen, the top of the valence band and the bottom of the conduction band touch at the Dirac point. There are two saddle points at the energies about ± 2.8, leading to the Van Hove singularities in the density of states. As the chemical potential is zero, the Fermi level is located at the Dirac points. Then the Fermi surface shrinks to points thus usually the superconductivity cannot occur. We add a chemical potential term (for doped graphene materials) into the system to pull the Fermi level away from the Dirac points. The Fermi surfaces of the system for different chemical potentials are shown in Fig. 1(b). As the chemical potential is small, there are six disconnected

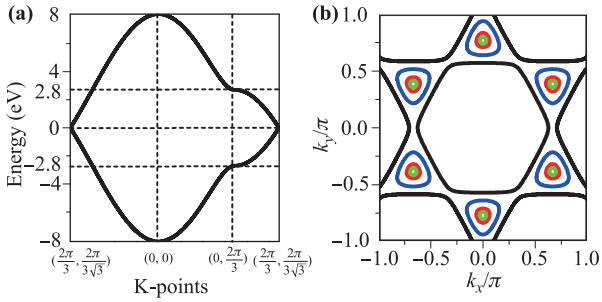

Fig. 1 **(a)** The normal state energy bands along the highly symmetrical lines in the Brillouin zone. **(b)** The normal state Fermi surfaces. From small to large pockets, the chemical potentials are 0.4, 0.8, 1.8, 2.8.

Fermi pockets. The pockets become large when the chemical potential increases. When the Fermi level is doped to near the saddle point, the Fermi pockets connect and the Fermi surface becomes a large pocket centered around the Brillouin zone center.

We now study the impurity effect for the $p+ip$ pairing symmetry. The LDOS spectra at the nearest-neighbour site of the impurity with different impurity scattering potentials and chemical potentials are plotted in Fig. 2. As the doping density is small, as is seen in Figs. 2(a–c), no in-gap resonances exist and the intensities of the superconducting coherent peaks are suppressed as the impurity strength increases. The most prominent feature revealed here is the existence of the in-gap resonant peaks when the Fermi energy reaches the Van Hove singularities, as presented in Fig. 2(d). At this doping level, two sharp in-gap resonant peaks emerge and the resonant peaks are lying symmetrically with respect to the Fermi energy due to the particle-hole symmetry of the superconducting Hamil-

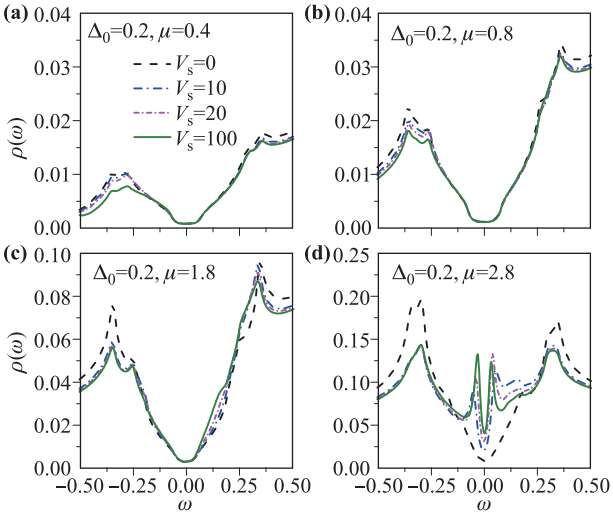

Fig. 2 The LDOS spectra at the nearest-neighbour site of the impurity for the $p+ip$ pairing symmetry.

tonian. Note that their strengths are nearly as strong as those of coherent peaks.

Let us discuss the impurity effect for the $d + id$ pairing symmetry. The corresponding LDOS spectra are presented in Fig. 3. Here U-shaped spectra are obtained for the case of $V_s = 0$, indicating that the system is nodeless. The energies of the superconducting coherent peaks are larger compared to those of the $p + ip$ pairing symmetry. The larger effective gap indicates that the $d + id$ pairing symmetry may be more suitable for the graphene-based energy band, and may have the lower free energy at the mean-field level, consistent with previous theoretical predictions [15–19]. The impurity induced in-gap states for the $d + id$ pairing symmetry are also clearly revealed. As the impurity strength increases, the in-gap states shift to near the Fermi energy. For the case of the highly doped compound ($\mu = 2.8$), the intensities of the in-gap peaks are significantly enhanced, qualitatively consistent with previous numerical calculations [31]. Obviously such strong in-gap features are the resonant states, and their intensities are much larger than that of the superconducting coherent peaks, thus it may be easily detected.

We turn to study the impurity effect for the extended s-wave pairing symmetry and the f-wave pairing symmetry, respectively. For both the extended s-wave pairing and the f-wave pairing, the effective gap magnitude becomes rather small, especially for tiny Fermi pockets when the chemical potential is small. Thus we would like to consider a larger input gap magnitude Δ_0 to obtain a large enough effective energy gap. In the following presented results, we set $\Delta_0 = 0.7$ for the cases of $\mu = 0.4$ and 0.8, and $\Delta_0 = 0.4$ for the cases of $\mu = 1.8$ and $\mu = 2.8$.

The numerical results for the impurity effect with the extended s-wave pairing symmetry are displayed in Fig. 4. Here the LDOS spectra are U-shaped thus the system is fully gapped. As the impurity scattering potential becomes larger, the superconducting coherent peaks are suppressed due to the impurity scattering. Note that, here for all of the parameters we considered, no in-gap resonant peaks exist, which is significantly different from the cases of the $d + id$ pairing symmetry. The numerical results for the case of the f-wave pairing symmetry are presented in Fig. 5. Generally the numerical results are qualitatively the same with those of extended s-wave pairing, except that for the case of the f-wave pairing, the system is nodal.

We here provide a physical picture accounting for the possible in-gap states of the $p + ip$ and $d + id$ pairing symmetries, through analyzing the superconducting order parameter near the Fermi surface. The superconducting gap

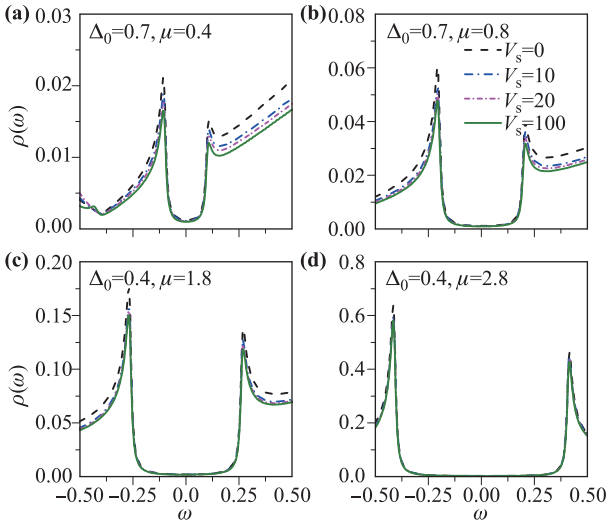

Fig. 4 The LDOS spectra at the nearest-neighbour site of the impurity for the extended s-wave pairing symmetry.

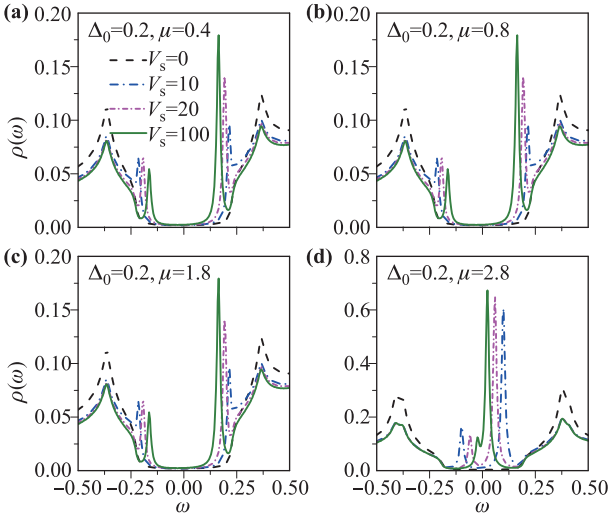

Fig. 3 The LDOS spectra at the nearest-neighbour site of the impurity for the $d + id$ pairing symmetry.

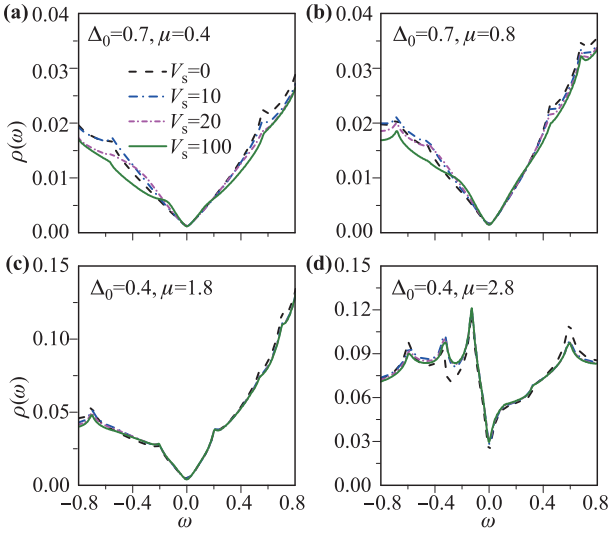

Fig. 5 The LDOS spectra at the nearest-neighbour site of the impurity for the f-wave pairing symmetry.

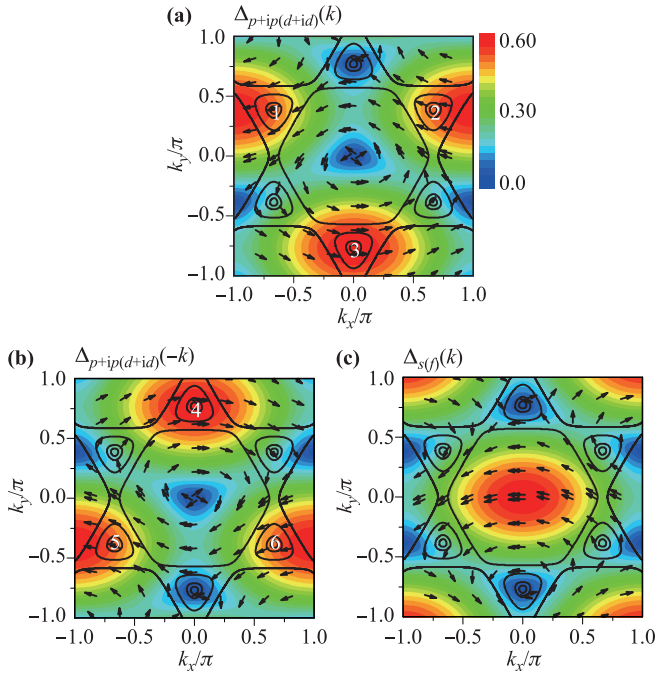

Fig. 6 The intensity plots of superconducting gap magnitude. The arrows indicate their phases. The solid lines are the replots of the normal state Fermi surfaces shown in Fig. 1(b).

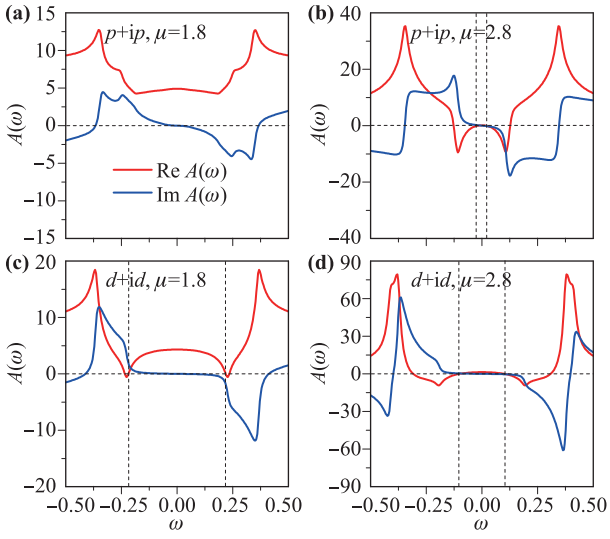

Fig. 7 The real and imaginary parts of the denominator of the T-matrix for the $p+ip$ and $d+id$ pairing symmetries with $\Delta_0 = 0.2$ and $V_s = 10$.

magnitudes and their phases [from Eq. (5)] are plotted in Fig. 6. As is seen in Figs. 6(a) and (b), for the $p+ip$ and $d+id$ pairing symmetries, the maximum superconducting gap is just near the normal state Fermi pockets, indicated by pockets $1-6$. The phases of the superconducting gap almost keep the same in one pocket and the phases are reversed for the pockets 1/2 and 3 (or pockets 5/6 and 4). Such sign reversal behavior is similar to the cases of the iron-based superconductors. Therefore, here the physical origin of the in-gap states is the same with the case in the iron-based superconductor [27, 28], which is suggested to be caused by the Andreev reflection due to the opposite phases of the order parameters [25]. For the case of the s-wave and f-wave pairing states, as is seen in Fig. 6(c), the maximum gap is always far away from the Fermi surface, as a result, the effective superconducting gap magnitudes are much smaller. And the phases of the gap are in disorder thus no in-gap resonant peaks exist.

The phase analysis and the sign reversal picture can explain qualitatively the emergence of the in-gap bound states. While the sign reversal of the order parameters is usually not the sufficient condition for the bound states. An alternative method to explain the the impurity induced resonant peaks can be achieved through discussing the denominator of the T-matrix $[A(\omega)]$ from Eq.7 with $A(\omega) = \mid \hat{I} - \hat{U}_0 \frac{1}{N} \sum_{\boldsymbol{k}} \hat{G}_0(\boldsymbol{k}, \omega) \mid$. Its imaginary part $[\mathrm{Im}A(\omega)]$ at the low energy is usually rather small due to the existence of the superconducting gap. A resonance will occur if its real part $[\mathrm{Re}A(\omega)]$ approaches to zero at a certain low energy. The denominator of the T-matrix with the $p+ip$ and $d+id$ pairing symmetries are presented in Fig. 7. As is seen, its imaginary part at low energies is indeed rather small. Then a resonance will occur if its real part approaches to zero. For the case of the $p+ip$ pairing symmetry, as the chemical potential is small ($\mu = 1.8$), as is seen in Fig. 7(a), the real part of the denominator does not approach to the zero value for all of the energies we considered. Therefore, at this doping level no in-gap bound states exist. When the chemical potential increases to $\mu = 2.8$, as is seen in Fig. 7(b), $\mathrm{Re}A(\omega)$ crosses the zero axis at two symmetrical low energies, as a result, the in-gap bound states emerge at these two energies. For the case of the $d+id$ pairing symmetry, as is seen in Figs. 7(c) and (d), $\mathrm{Re}A(\omega)$ crosses the zero axis for both two chemical potentials we considered. Therefore, the in-gap bound states emerge. Moreover, since the spectra for the $d+id$ pairing is fully gapped and the effective gap magnitudes are larger, the imaginary parts of the denominator $[\mathrm{Im}A(\omega)]$ are rather small. As a result, the intensity of the in-gap peaks for the $d+id$ pairing symmetry are rather strong and may be detected easily.

Finally, we discuss whether different pairing states can be resolved from the LDOS near a single impurity. For the cases of the $p+ip$ and $d+id$ pairing symmetries, at highly doping level where the Fermi level is close to the Van Hove singularities, there exist in-gap resonant peaks induced by the impurity. However, the spectra for the $d+id$ pairing symmetry is fully gapped and the in-gap resonant peaks for the $d+id$ pairing symmetry are much stronger than that for the $p+ip$ pairing symmetry. For the cases of the extended s-wave and f-wave pairing symmetries, there are no in-gap states, and the spectra for the s-wave pairing symmetry are fully gapped and those for the f-wave one

are nodal. Obviously, at low doping levels, the $d + id$ pairing symmetry is different from other three ones, i.e., there exist strong in-gap peaks for the case of the $d + id$ pairing symmetry. Therefore, we conclude that, the impurity effect indeed provides some useful information and the pairing symmetry may be resolved at some typical doping levels. Especially, the $d+id$ pairing symmetry may be distinguished from other three pairing symmetries.

4 Summary

In summary, we have studied theoretically the single impurity effect of graphene-based superconductors. Four different pairing symmetries, i.e., the $p+ip$ pairing, the $d+id$ pairing, the extended s-wave pairing and the f-wave pairing, are considered. Robust in-gap resonant states are revealed for the $d + id$ pairing symmetry. For the $p + ip$ pairing symmetry, the in-gap resonant states are sensitive to the doping level and they exist at the highly doped sample. For the f-wave and extended s-wave pairing symmetries, no in-gap resonant states are obtained for all of the parameters we considered. All of the features can be explained through analyzing the order parameter along the Fermi pockets and the denominator of the T-matrix. We conclude that the impurity effect may provide useful information to resolve different pairing symmetries in graphene-based superconductors.

Acknowledgements This work was supported by the National Natural Science Foundation of China (Grant No. 12074130) and the Science and Technology Program of Guangzhou Province (Grant No. 2019050001).

References

1. A. H. Castro Neto, F. Guinea, N. M. R. Peres, K. S. Novoselov, and A. K. Geim, The electronic properties of graphene, *Rev. Mod. Phys.* 81(1), 109 (2009)
2. K. S. Novoselov, D. V. Andreeva, W. Ren, and G. Shan, Graphene and other two-dimensional materials, *Front. Phys.* 14(1), 13301 (2019)
3. C. Tonnoir, A. Kimouche, J. Coraux, L. Magaud, B. Delsol, B. Gilles, and C. Chapelier, Induced superconductivity in graphene grown on rhenium, *Phys. Rev. Lett.* 111(24), 246805 (2013)
4. S. Ichinokura, K. Sugawara, A. Takayama, T. Takahashi, and S. Hasegawa, Superconducting calcium-intercalated bilayer graphene, *ACS Nano* 10(2), 2761 (2016)
5. J. Chapman, Y. Su, C. A. Howard, Dmytro Kundys, A. N. Grigorenko, F. Guinea, A. K. Geim, I. V. Grigorieva, and R. R. Nair, Superconductivity in Ca-doped graphene laminates, *Sci. Rep.* 6(1), 23254 (2016)
6. B. M. Ludbrook, G. Levy, P. Nigge, M. Zonno, M. Schneider, D. J. Dvorak, C. N. Veenstra, S. Zhdanovich, D. Wong, P. Dosanjh, C. Straßer, A. Stohr, S. Forti, C. R. Ast, U. Starke, and A. Damascelli, Evidence for superconductivity in Li-decorated monolayer graphene, *Proc. Natl. Acad. Sci. USA* 112(38), 11795 (2015)
7. A. Di Bernardo, O. Millo, M. Barbone, H. Alpern, Y. Kalcheim, U. Sassi, A. K. Ott, D. De Fazio, D. Yoon, M. Amado, A. C. Ferrari, J. Linder, and J. W. A. Robinson, p-wave triggered superconductivity in single-layer graphene on an electron-doped oxide superconductor, *Nat. Commun.* 8(1), 14024 (2017)
8. Y. Cao, V. Fatemi, S. Fang, K. Watanabe, T. Taniguchi, E. Kaxiras, and P. Jarillo-Herrero, Unconventional superconductivity in magic-angle graphene superlattices, *Nature* 556(7699), 43 (2018)
9. B. Uchoa and A. H. Castro Neto, Superconducting states of pure and doped graphene, *Phys. Rev. Lett.* 98(14), 146801 (2007)
10. N. B. Kopnin and E. B. Sonin, BCS superconductivity of Dirac electrons in graphene layers, *Phys. Rev. Lett.* 100(24), 246808 (2008)
11. J. Linder, A. M. Black-Schaffer, T. Yokoyama, S. Doniach, and A. Sudbø, Josephson current in graphene: Role of unconventional pairing symmetries, *Phys. Rev. B* 80(9), 094522 (2009)
12. A. M. Black-Schaffer and S. Doniach, Possibility of measuring intrinsic electronic correlations in graphene using a d-wave contact Josephson junction, *Phys. Rev. B* 81(1), 014517 (2010)
13. T. Ma, F. Yang, H. Yao, and H. Q. Lin, Possible triplet $p + ip$ superconductivity in graphene at low filling, *Phys. Rev. B* 90(24), 245114 (2014)
14. J. P. L. Faye, P. Sahebsara, and D. Senechal, Chiral triplet superconductivity on the graphene lattice, *Phys. Rev. B* 92(8), 085121 (2015)
15. T. Ma, Z. Huang, F. Hu, and H. Q. Lin, Pairing in graphene: A quantum Monte Carlo study, *Phys. Rev. B* 84(12), 121410 (2011)
16. R. Nandkishore, L. S. Levitov, and A. V. Chubukov, Chiral superconductivity from repulsive interactions in doped grapheme, *Nat. Phys.* 8(2), 158 (2012)
17. M. L. Kiesel, C. Platt, W. Hanke, D. A. Abanin, and R. Thomale, Competing many-body instabilities and unconventional superconductivity in grapheme, *Phys. Rev. B* 86(2), R020507 (2012)
18. R. Nandkishore, R. Thomale, and A. V. Chubukov, Superconductivity from weak repulsion in hexagonal lattice systems, *Phys. Rev. B* 89(14), 144501 (2014)
19. L. Y. Xiao, S. L. Yu, W. Wang, Z. J. Yao, and J. X. Li, Possible singlet and triplet superconductivity on honeycomb lattice, *Europhys. Lett.* 115(2), 27008 (2016)
20. M. V. Hosseini and M. Zareyan, Model of an exotic chiral superconducting phase in a graphene bilayer, *Phys. Rev. Lett.* 108(14), 147001 (2012)
21. J. L. Lado and J. Fernandez-Rossier, Unconventional Yu–Shiba–Rusinov states in hydrogenated grapheme, *2D Mater.* 3(2), 025001 (2016)
22. T. Huang, L. Zhang, and T. Ma, Antiferromagnetically ordered Mott insulator and $d + id$ superconductivity in twisted bilayer graphene: A quantum Monte Carlo study, *Sci. Bull. (Beijing)* 64(5), 310 (2019)

23. W. Chen, Y. Chu, T. Huang, and T. Ma, Metal-insulator transition and dominant $d + id$ pairing symmetry in twisted bilayer graphene, *Phys. Rev. B* 101(15), 155413 (2020)
24. C. X. Zhao and J. F. Jia, Stanene: A good platform for topological insulator and topological superconductor, *Front. Phys.* 15(5), 53201 (2020)
25. C. R. Hu, Midgap surface states as a novel signature for $d_{x_{a^2}-x_{b^2}}$-wave superconductivity, *Phys. Rev. Lett.* 72(10), 1526 (1994)
26. A. V. Balatsky, I. Vekhter, and J. X. Zhu, Impurity-induced states in conventional and unconventional superconductors, *Rev. Mod. Phys.* 78(2), 373 (2006)
27. D. G. Zhang, Nonmagnetic impurity resonances as a signature of sign-reversal pairing in FeAs-based superconductors, *Phys. Rev. Lett.* 103(18), 186402 (2009)
28. W. F. Tsai, Y. Y. Zhang, C. Fang, and J. P. Hu, Impurity-induced bound states in iron-based superconductors with s-wave $\cos(kx) \cdot \cos(ky)$ pairing symmetry, *Phys. Rev. B* 80(6), 064513 (2009)
29. D. D. Wang, B. Liu, M. Liu, Y. F. Yang, and S. P. Feng, Impurity-induced bound states as a signature of pairing symmetry in multiband superconducting $CeCu_2Si_2$, *Front. Phys.* 14(1), 13501 (2019)
30. F. M. D. Pellegrino, G. G. N. Angilella, and R. Pucci, Pairing symmetry of superconducting graphene, *Eur. Phys. J. B* 76(3), 469 (2010)
31. T. O. Wehling, H. P. Dahal, A. I. Lichtenstein, and A. V. Balatsky, Local impurity effects in superconducting graphene, *Phys. Rev. B* 78(3), 035414 (2008)
32. O. A. Awoga and A. M. Black-Schaffer, Probing unconventional superconductivity in proximitized graphene by impurity scattering, *Phys. Rev. B* 97(21), 214515 (2018)
33. E. W. Hudson, S. H. Pan, A. K. Gupta, K.-W. Ng, and J. C. Davis, Atomic-scale quasi-particle scattering resonances in $Bi_2Sr_2CaCu_2O_{8+\delta}$, *Science* 285(5424), 88 (1999)
34. D. K. Morr, Resonant impurity states in the d-density-wave phase, *Phys. Rev. Lett.* 89(10), 106401 (2002)
35. N. Andrenacci, G. G. N. Angilella, H. Beck, and R. Pucci, Linear response theory around a localized impurity in the pseudogap regime of an anisotropic superconductor: Precursor pairing versus d-density-wave scenario, *Phys. Rev. B* 70(2), 024507 (2004)
36. M. M. Scherer, Graphene doping reaches new levels, *Physics (College Park Md.)* 13, 161 (2020)
37. P. Rosenzweig, H. Karakachian, D. Marchenko, K. Küster, and U. Starke, Overdoping graphene beyond the van hove singularity, *Phys. Rev. Lett.* 125(17), 176403 (2020)
38. T. Löthman and A. M. Black-Schaffer, Defects in the $d+id$-wave superconducting state in heavily doped graphene, *Phys. Rev. B* 90(22), 224504 (2014)